# Groove-type channel enhancement-mode AlGaN/GaN MIS HEMT with combined polar and nonpolar AlGaN/GaN heterostructures*

Xiao-Ling Duan(段小玲), Jin-Cheng Zhang(张进成)†, Ming Xiao(肖明), Yi Zhao(赵一), Jing Ning(宁静), and Yue Hao(郝跃)

*Key Laboratory of Wide Band-Gap Semiconductor Technology, School of Microelectronics, Xidian University, Xi'an* 710071, *China*

(Received 26 January 2016; revised manuscript received 31 March 2016; published online 25 June 2016)

A novel groove-type channel enhancement-mode AlGaN/GaN MIS high electron mobility transistor (GTCE-HEMT) with a combined polar and nonpolar AlGaN/GaN heterostucture is presented. The device simulation shows a threshold voltage of 1.24 V, peak transconductance of 182 mS/mm, and subthreshold slope of 85 mV/dec, which are obtained by adjusting the device parameters. Interestingly, it is possible to control the threshold voltage accurately without precisely controlling the etching depth in fabrication by adopting this structure. Besides, the breakdown voltage ($V_B$) is significantly increased by 78% in comparison with the value of the conventional MIS-HEMT. Moreover, the fabrication process of the novel device is entirely compatible with that of the conventional depletion-mode (D-mode) polar AlGaN/GaN HEMT. It presents a promising way to realize the switch application and the E/D-mode logic circuits.

**Keywords:** AlGaN/GaN HEMT, enhancement-mode operation, groove-type channel, nonpolar

**PACS:** 73.40.Kp, 85.30.De, 85.30.Tv **DOI:** 10.1088/1674-1056/25/8/087304

## 1. Introduction

GaN-based electronic devices have attracted more and more attention due to their excellent material properties such as high saturation electron velocities and breakdown electric fields.[1,2] Most of the reported AlGaN/GaN high electron mobility transistors (HEMTs) show D-mode operation because the two-dimensional electron gas (2DEG) exists at the heterointerface at a gate bias voltage of 0 V.[3] However, E-mode operation is essential for the safe operation of power electronic applications and the realization of various monolithic integrated enhancement-/depletion-mode (E/D-mode) digital circuits.

So far, several techniques for achieving the enhancement-mode (E-mode) operation in the AlGaN/GaN HEMTs have been reported, such as gate recess, fluoride-based plasma treatment, reducing the composition or the thickness of the AlGaN barrier, and a nonpolar *a*-plane channel. However, in the above techniques some problems still exist. Gate-recess is a viable approach;[4] but the threshold voltage cannot be easily reproduced by the dry etching technique, because the polarization charge density is highly dependent on the recess depth.[5] Another approach to fluoride-based plasma treatment may degenerate the device uniformity and make the devices very unstable.[6,7] As a part of the epitaxial design, the decreasing of the composition or the thickness of the AlGaN[8,9] to reduce the sheet charge can achieve the E-mode operation, but the increase of parasitic resistance between the source and the drain is difficult to overcome. As the above technique difficulties all arise from the purpose of reducing two-dimensional electron gas (2DEG) under the gate in polar AlGaN/GaN, the nonpolar AlGaN/GaN HEMT that is free from the polarization-induced sheet charges has attracted attention and been demonstrated with E-mode operation in recent years.[10–12] Some techniques such as Si $\delta$-doping,[13] regrown $n^+$-GaN contact layer,[14] and $Al_2O_3$ gate dielectric[15] have been adopted to improve the performance of nonpolar GaN-based HEMT. However, its maximum transconductance and maximum current density are still low compared with E-mode AlGaN/GaN HEMT on *c*-plane GaN. Thus, combining the advantages of the polar and nonpolar heterostructure to realize E-mode operation is expected to be a promising method to solve this problem. However, to the best of our knowledge, both the design and the fabrication of structure based on this concept have not been discussed so far.

In this paper, a novel device structure called groove-type channel enhancement-mode AlGaN/GaN MIS HEMT (GTCE-HEMT) is presented, in which the recess etching and regrowth technology are adopted to realize the combination of the polar and nonpolar AlGaN/GaN heterostructure. These technologies are widely used in the fabrication process,[16–18] especially in the fabrication of the vertical GaN HEMT.[19–21] Therefore, the fabrication process of the GTCE-HEMT is compatible with that of the conventional D-mode devices. In this paper, we analyze the physical mechanism of the GTCE-HEMT to realize E-mode operation, and the influence of gate recess depth on the direct current (DC) characteristics, and

*Project supported by the National Science and Technology Major Project, China (Grant No. 2013ZX02308-002) and the National Natural Science Foundation of China (Grant Nos. 11435010, 61474086, and 61404099).

†Corresponding author. E-mail: jchzhang@xidian.edu.cn

© 2016 Chinese Physical Society and IOP Publishing Ltd 

then we investigate the mechanism of the GTCE-HEMT to improve the breakdown voltage by two-dimensional (2D) numerical simulations. The simulations show excellent device performances. Interestingly, by using the groove channel, the breakdown voltage ($V_B$) is successfully increased compared with that of the conventional MIS-HEMT. Moreover, the $V_{th}$ has a saturation value as the recess depth is beyond 500 nm. That is to say, when the recess depth reaches about 500 nm, a continued process of recessing has almost no effect on $V_{th}$. Therefore, the GTCE-HEMT can avoid the difficulty in controlling the threshold voltage by dry etching technique and improve the threshold voltage uniformity. In addition, the fabrication process of the GTCE-HEMT is compatible with that of the conventional D-mode devices.

## 2. Device structure and physical models

The GTCE-HEMT structure is proposed and schematically shown in Fig. 1. It includes a 500-nm p-doped *c*-plane GaN buffer layer, a 600-nm unintentionally doped (UID) GaN layer with a recessed gate, followed by a 100-nm UID regrown GaN channel and $Al_{0.3}Ga_{0.7}N$ barrier layer on the recessed GaN layer. The cross section of AlGaN/GaN heterointerface is of a groove type. The heterostructures outside and at the bottom of the groove are polar-plane, which grows along the (0001) orientation; the sidewall of the groove is nonpolar-plane, the growth direction of which is perpendicular to the (0001) direction. The nonpolar-plane heterostructure is not affected by polarization-induced charges since the polarization field is not formed perpendicularly to the nonpolar-plane.[10,11] Therefore, 2DEG exists at the *c*-plane heterostructure (the channel except for the sidewalls of the groove), but almost no 2DEG is formed at the interface of the nonpolar AlGaN/GaN heterostructure. This induces the E-mode operation and a larger maximum drain current. The relevant design parameters used in the SILVACO-ATLAS simulations are listed in Table 1.

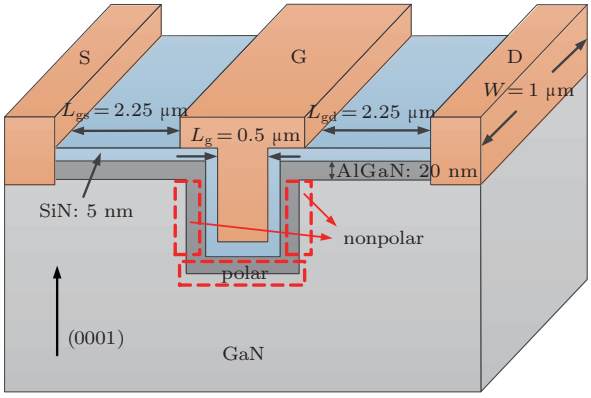



**Fig. 1.** (color online) The schematic diagram of GTCE-HEMT in the ATLAS simulator.

**Table 1.** Required characteristic for designing the GTCE-HEMT.

| Parameter | Value |
|---|---|
| Gate length, $L_g$/μm | 0.5 |
| Gate–source spacing, $L_{gs}$/μm | 2.25 |
| Gate–drain spacing, $L_{gd}$/μm | 2.25 |
| Recess etching depth, $t$/nm | 0, 100, 200, 300,400, 500 |
| *c*-plane AlGaN thickness/nm | 20 |
| Lateral growth nonpolar AlGaN thickness, $d_{AlGaN}$/nm | 15 |
| Gate dielectric $SiN_x$ thickness, $d_{SiN}$/nm | 5 |
| Source/drain doping concentration/$cm^{-3}$ | $1\times10^{19}$ |
| GaN channel layer background concentration, $n$/$cm^{-3}$ | $1\times10^{15}$ (Ref. [22]) |
| GaN buffer layer p-doped concentration, $p$/$cm^{-3}$ | $5\times10^{16}$ |
| Gate metal work function, WF/eV | 5.2 (Ref. [23]) |
| 2DEG density, $n_{2DEG}$/$cm^{-3}$ | $1\times10^{13}$ (Ref. [22]) |
| Low field electron mobility of polar GaN/($cm^2$/V·s) | 900 (Ref. [23]) |
| Low field electron mobility of nonpolar GaN/($cm^2$/V·s) | 50 (Ref. [10]) |
| Low field electron mobility of AlGaN/($cm^2$/V·s) | 100 |
| $V_{sat}$ of GaN/cm·$s^{-1}$ | $1.91\times10^7$ (Ref. [24]) |
| $V_{sat}$ of AlGaN/cm·$s^{-1}$ | $1.12\times10^7$ (Ref. [24]) |

The analysis of the GaN-based HEMT in this paper is performed by SILVOCAL-ATLAS software. The positive sheet charge with a density of $1\times10^{13}$ $cm^{-2}$ at the interface between polar AlGaN and GaN is used to model the positive polarization charge.[22] Meanwhile, the fixed sheet charge along the nonpolar plane heterointerface is designed to be zero. Acceptor traps with a density of $1\times10^{15}$ $cm^{-3}$ located at 0.5 eV below the conduction band edge are employed in the buffer layer to model the carbon atomic pollution during the growth.[25] The Shockley–Read–Hall (SRH) carrier recombination model, constant low field mobility model, field-dependent mobility model at high electric fields, and the impact ionization model

are used in the simulation study.[26] The low field electron mobility is designed to be 900 $cm^2/V{\cdot}s$ and 50 $cm^2/V{\cdot}s$ in the polar GaN region and nonpolar GaN region (the GaN region near the nonpolar AlGaN/GaN interface),[10,11,23] respectively. The impact ionization for GaN is described as $\alpha_0 \exp(-E_C/E)$ with $\alpha_0 = 2.9 \times 10^8$/cm, and $E_C = 3.4 \times 10^7$ V/cm. All the simulations are carried out at the room temperature of 300 K. Under these conditions, the DC characteristics of the GTCE-HEMT are simulated and analyzed.

Figure 2 shows a fabrication flow chart of the GTCE-HEMT. The process starts with GaN epitaxial layer growth over a *c*-plane sapphire structure at stage 1. Then, the GaN layer in the gate region is etched by reactive ion etching (RIE) using a $BCl_3/Cl_2$ gas mixture, followed by tetramethylammonium hydroxide treatment for the removal of the roughness of the dry etched GaN surface[27,28] at stage 2. Stage 3 includes the regrowth of AlGaN/GaN heterostructure by molecular beam epitaxy (MBE). Prior to the regrowth process, the template is cleaned with standard RCA clean and further by *in situ* alternating vacuum thermal dissociation and GaN regrowth cycles.[29] The regrown epilayer consists of, first, 100-nm-thick GaN on the recessed GaN template and, subsequently, a 20-nm-thick $Al_{0.3}Ga_{0.7}N$ barrier layer, thus smooth AlGaN/GaN interfaces and the better electron transport channel can be expected.[30] The final stage includes device isolation, Ohmic electrode deposition, gate dielectric layer deposition, and gate metal electrode deposition, the same as the procedure done for the conventional HEMT.

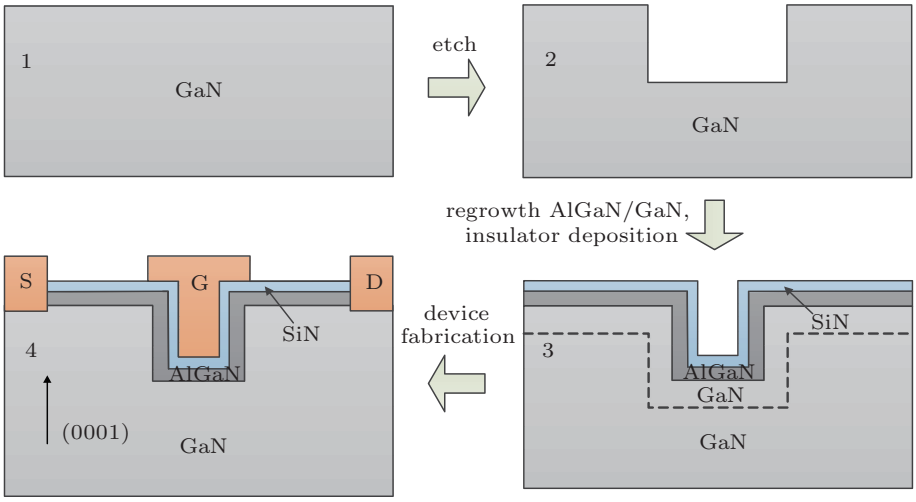



**Fig. 2.** (color online) Fabrication flow chart of GTCE-HEMT.

## 3. Results and discussion

### 3.1. Physical mechanism

#### 3.1.1. Physics of the polar and nonpolar AlGaN/GaN heterostructures

The natural structure of the III–V nitrides is wurtzite, a noncentrosymmetrical structure with polar axis, namely the *c* axis. The centers of positive and negative charges do not coincide in the equilibrium lattice of the III–nitrides at zero strain, hence inducing the spontaneous polarization along the polar axis.[31,32] Furthermore, with an applied stress, the lattice deformation induces a separation of the centers of the positive and negative charges in the crystal, thus forming dipole moments, the accumulation of which leads to the polarization charges on the crystal surface. This additional polarization in strained III–nitrides crystal is called piezoelectric polarization.[31–33]

In the (0001) plane AlGaN/GaN heterostructures, the spontaneous polarization occurs along the $[000\bar{1}]$ direction; the piezoelectric polarization in the AlGaN layer is in the same direction as the piezoelectric polarization direction. The polarization gives rise to a strong build-in electric field on the order of MV/cm along the growth axis and polarization bound charges with a density of $1\times10^{13}$ $cm^{-2}$ at the interface, which have been shown to modulate the energy band of the heterostructures and influence mobile carrier distributions. The positive bound charges will attract electrons at the interface between the two layers, thereby inducing the 2DEG (which is formed without any intentional doping).[31,34,35] To achieve high 2DEG mobility, the interface at AlGaN/GaN heterostructures must be laterally smooth and the composition transition is vertically abrupt. Fortunately, up to now, the AlGaN/GaN heterostructures have widely been investigated and found to have good material characteristics, such as the smooth interface, low dislocations and the high confinement of 2DEG. For well-confined 2DEG, defects, such as ionized impurities or dislocations can be effectively screened and contribute less to the overall scattering. Besides, most of the studied AlGaN/GaN heterostructures are undoped, thus having no ionized dopants scattering. From the above, the 2DEG in polar heterostructures is in the nature of the high electron

mobility.[36]

For the nonpolar AlGaN/GaN, the crystal orientation is perpendicular to the polar axis, hence it is not affected by the polarization effect. In the undoped nonpolar heterostructure, no 2DEG is formed at the interface. This characteristic can be used to realize the E-mode operation. However, recent reports show that the electron mobility of the nonpolar heterostructure is still very low. One possible reason for the low mobility is the rough interface of the nonpolar heterostructure. The root mean square surface roughness is 2.8 nm on *a*-plane AlGaN/GaN measured by an atomic force microscope, as reported by Chang *et al.*[37] It is much larger than the root mean square surface roughness of 0.3 nm on the (0001) plane heterostructures. Besides, many dislocations in the nonpolar material also affect the electron mobility. As Kuroda *et al.*[10] reported, the density of the threading dislocations in the *a*-plane GaN is more than $10^{10}$ cm$^{-2}$, which is much higher than $10^{9}$ cm$^{-2}$ in the *c*-plane GaN. Therefore, controlling the growth process to substantially improve the quality of the nonpolar crystal will be an important work to improve the electron mobility. In this paper, we just use the nonpolar materials at the sidewalls of the groove channel, thus significantly reducing the drawbacks of the nonpolar heterostructures.

### 3.1.2. Working principle of the device

The 2DEG density and the energy band diagrams of the proposed GTCE-HEMT under different bias conditions are shown in Fig. 3.

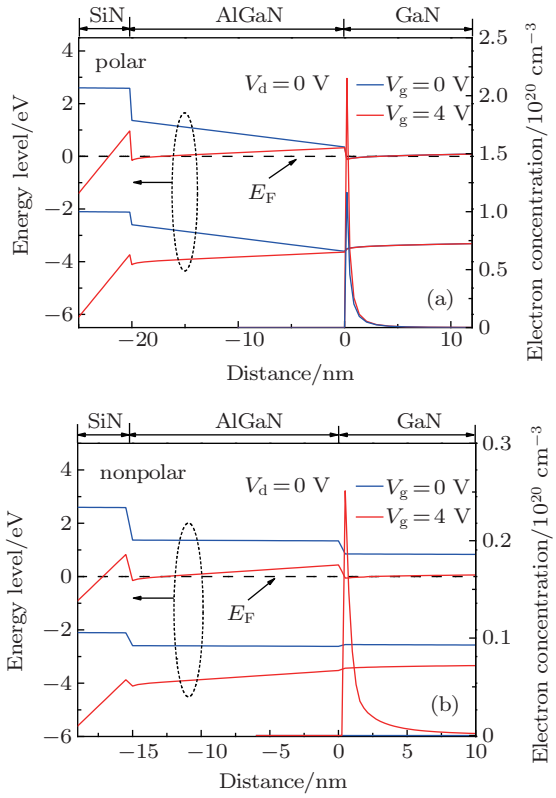



**Fig. 3.** (color online) Energy band diagram and electron density (a) underneath the gate region (polar AlGaN/GaN) and (b) on the sidewall of the groove (nonpolar AlGaN/GaN ) with $V_g = 0$ V and 4 V at $V_d = 0$ V.

The conduction band in the polar GaN region near the interface of the AlGaN/GaN heterostructure underneath the gate region is lower than the Fermi level $E_F$ even as no voltage is applied, which indicates the existence of 2DEG in the potential well as shown in Fig. 3(a). However, the energy band of the nonpolar AlGaN/GaN heterostructure on the sidewall of the groove is different from that of the polar-plane. As shown in Fig. 3(b), the conduction band is higher than the $E_F$ when no voltage is applied, thus, there is no 2DEG near the interface of the nonpolar-plane heterostucture. When the gate voltage exceeds the $V_{th}$, the conduction band in the GaN region near the interface of the nonpolar heterostructure falls below the $E_F$ with an accumulation of the carriers in the potential well in Fig. 3(b). At this moment, the groove channel forms and the device can work. Figure 4 shows the simulated electron concentrations in the GTCE-HEMT for the off-state condition and for the on-state condition in logarithmic coordinates respectively. It is obvious that there are no carriers on the sidewalls of the groove as no voltage is applied, so the channel is off. When $V_g = 4$ V and $V_d = 10$ V, a large number of electrons accumulate in the groove channel, including the sidewalls, so the device works, which is in accordance with the above discussion.

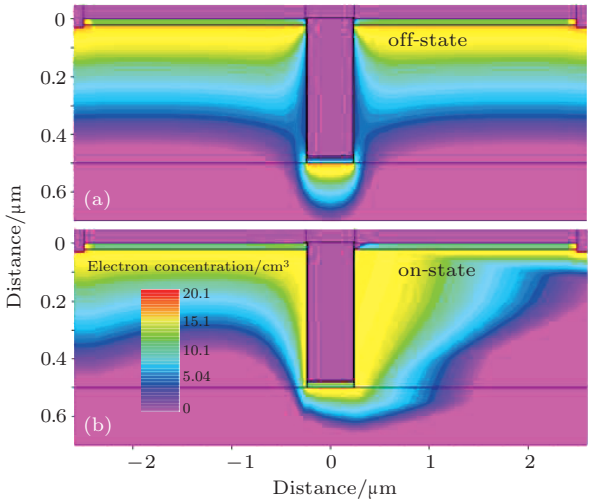



**Fig. 4.** (color online) Logarithmic electron concentrations in the GTCE-HEMT for (a) off-state condition ($V_g = 0$ V, $V_d = 0$ V) and for (b) on-state condition ($V_g = 4$ V, $V_d = 10$ V).

## 3.2. Influence of the gate recess depth

The gate recess depth is an important parameter in the ordinary gate-recessing HEMT, which affects the value of the threshold voltage, so discussion about the recess depth is necessary in this paper. Device models with various values of gate recess depth t are established to investigate the DC characteristics of the GTCE-HEMT with a gate metal work function of 5.2 eV. The thickness of $SiN_x$ and the nonpolar AlGaN are 5 nm and 15 nm, respectively. Figure 5(a) shows the transfer characteristics of the devices with different recess depths at $V_d = 10$ V. By defining the threshold voltage as the gate volt-

age axis intercept of linear extrapolation of the $I_d$–$V_g$ curve at the gate bias that produces the peak transconductance, the values of extracted threshold voltage ($V_{th}$) are −2.83 V, −0.35 V, 0.93 V, 1.17 V, 1.22 V, and 1.24 V for the 0 nm–500 nm recess depth in steps of 100 nm, respectively. As shown in Fig. 5(b), the $V_{th}$ shifts to the positive direction with $t$ increasing and becomes saturated at a certain recess depth, which means that an obvious variation of the recess depth (100 nm) has almost no effect on the threshold voltage (0.02 V). In the conventional gate recessed GaN-HEMT, the $V_{th}$ variation is expected to be about 2 V as the recess depth varies 10 nm.[38] This result indicates that the proposed structure can control the threshold voltage accurately without precisely controlling the recess depth in fabrication. Figure 5(b) also shows that the peak transconductance ($g_m$(max)) increases with the recess depth increasing from 0 nm to 300 nm, and then decreases with a continued process of etching. Besides, the subthreshold slope (SS) is shown in Fig. 5(c).

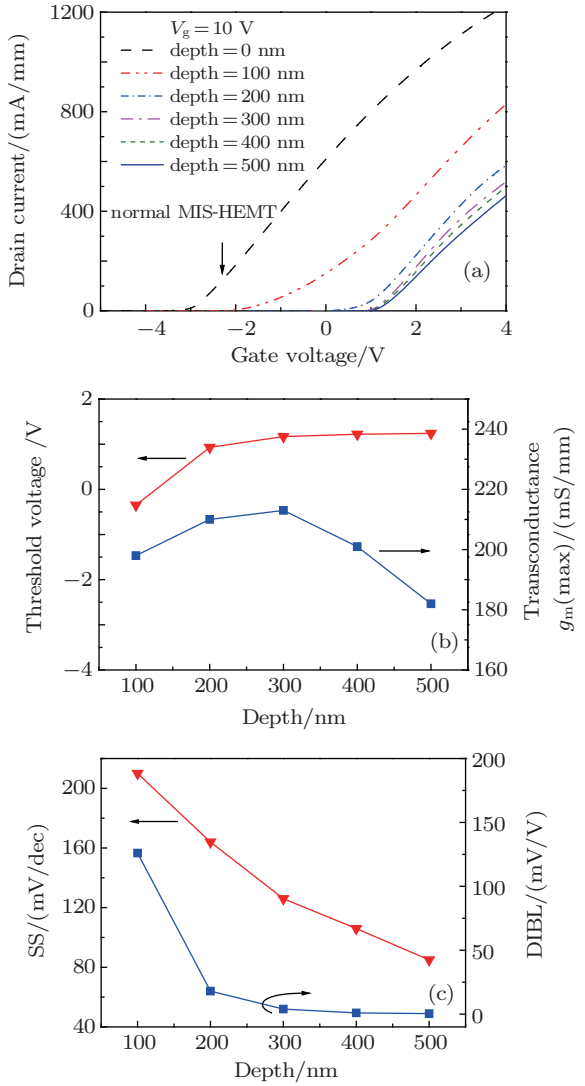



**Fig. 5.** (color online) (a) Transfer characteristics for different depths, (b) $V_{th}$ and transconductance characteristic, and (c) subthreshold slope and DIBL of the GTCE-HEMT each as a function of gate recess etching depth.

The DC characteristics of the devices with different recess depths can be explained by the short channel effect (SCE). As the channel at the bottom of the groove is always conductive under the normal switch condition, the sidewall of the groove channel near the source dominates the device characteristics. Thereby the effective gate length is actually the groove depth t, but not the horizontal gate length $L_g$. To mitigate the short-channel effects, the minimum aspect ratio ($t/t_{bar}$) of 15 is proposed.[39] Herein, $t_{bar} = d_{AlGaN} + d_{SiN}$. As $t_{bar}$ in this simulation is 20 nm, the recess depth should be larger than 300 nm. It means that short-channel effects such as the threshold voltage shift, transconductance decreasing, and the subthreshold slope deterioration may occur if the recess depth is lower than 300 nm. The conventional definition of the drain-induced barrier lowering (DIBL) (defined as $\Delta V_{th}/\Delta V_d$) is used to characterize the threshold voltage shift in HEMT. A plot of the simulated DIBL as a function of the recess depth is shown in Fig. 5(c). As the recess depth ranges from 500 nm to 300 nm, the DIBL just increases a little. Then the DIBL increases rapidly with the recess depth continually decreasing. When the recess depth decreases to 100 nm, the DIBL increases to 126 mV/V, since the channel control becomes worse with the aspect ratio decreasing. It is in accordance with the subthreshold slope degradation.

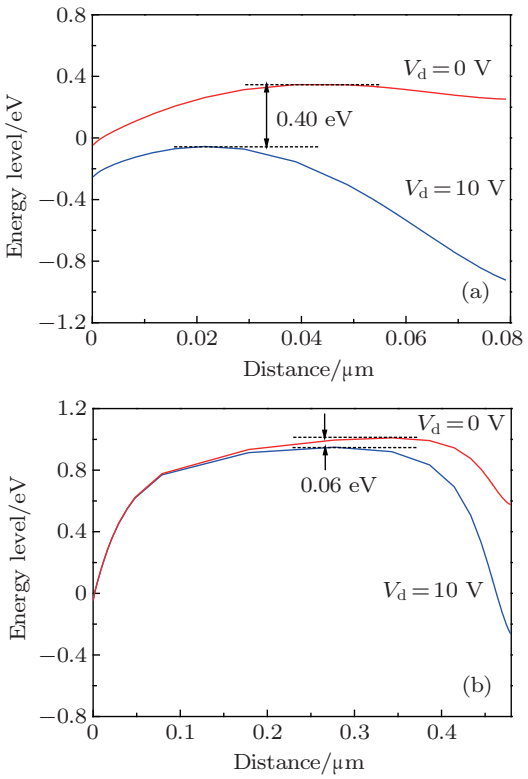



**Fig. 6.** (color online) Conduction band profiles along the channel of GTCE-HEMT for (a) 100 nm- and (b) 500-nm recess depth with different drain bias voltages.

In order to further investigate the DIBL effect, the potential barriers of the channel with different drain bias voltages at $V_g = 0$ V are simulated and the results are shown in Fig. 6. The

potential barrier is reduced by 0.40 eV for the device with a recess depth of 100 nm, which leads to the $V_{th}$ reduction and the DIBL. However, as the recess depth is 500 nm, the reduction of the potential barrier (0.06 eV) can be ignored even under a high drain bias. The gate can well control the potential barrier when the recess depth is larger than 300 nm. However, the performance of this device is seriously affected by SCE as the depth is below 300 nm. It has been well explained why the $g_m$ increases first and then decreases with the recess depth ranging from 500 nm to 100 nm.

### 3.3. Breakdown characteristic

In Fig. 7, we present the effect of the recess depth on the breakdown voltage ($V_B$). It shows that the $V_B$ increases markedly as the recess depth increases from 100 nm to 500 nm.

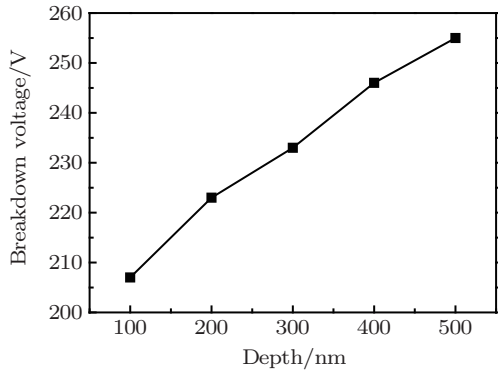



**Fig. 7.** Variation of breakdown voltage with recess depth.

To further investigate the breakdown characteristic of the GTCE-HEMT, a conventional MIS-HEMT with a planar channel is simulated as a referential sample by using the same channel length and other device parameters as the GTCE-HEMT. The device simulation shows that GTCE-HEMT enhances the breakdown characteristics successfully by managing the electric field profile in the channel. The $V_B$ is significantly increased by 78% from 143 V of the conventional MIS-HEMT (recess depth of 0 nm) to 255 V of the GTCE-HEMT (recess depth of 500 nm).

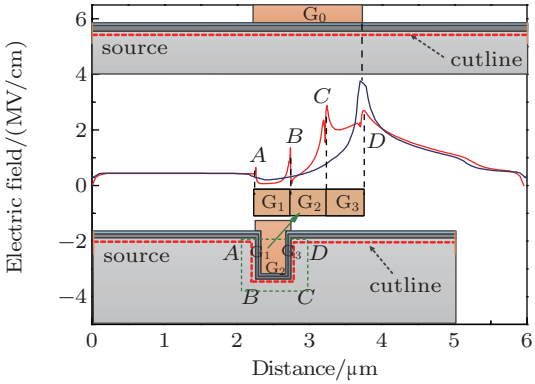



**Fig. 8.** (color online) Electric field distributions along the interface of AlGaN/GaN for GTCE-HEMT (red line) and the conventional device (blue line). The dash line is from the source to the drain.

The comparison in electric field distribution at the AlGaN/GaN interface between the 500-nm-recess depth GTCE-HEMT and the conventional MIS-HEMT is shown in Fig. 8. As can be seen, when the simulation is performed at $V_d$ = 200 V, the maximum value of the electric field for GTCE-HEMT is 2.9 MV/cm, while that of the conventional MIS-HEMT is 3.7 MV/cm. The breakdown happens at $V_d = 200$ V in the conventional device, as the value of the electric field peak has exceeded the critical electric field value of GaN (3.3 MV/cm).[40] Interestingly, GTCE-HEMT can work well. On the proposed structure, three extra electric field peaks occur in the electric field distribution. All the peaks are observed at the corners of the gate; *C* and *D* are two higher peaks located at the gate edge near the drain side due to the electric field crowding effect. It is worth noting that the recess gate has broadened the high-field region and effectively reduced the amount of the electric field crowded near the upper gate edge (peak *D*). Therefore, higher voltage is required in order to reach the critical electric field, which means that GTCE-HEMT can work at high voltage compared with the conventional structure. That is the reason why the GTCE-HEMT can improve the breakdown characteristics.

## 4. Conclusions

In this paper, we present a GTCE-HEMT that combines the polar and the nonpolar AlGaN/GaN heterostructure, and study its operation principle and DC characteristic by 2D simulations. A threshold voltage of 1.24 V, peak transconductance of 182 mS/mm, and subthreshold slope of 85 mV/dec are obtained by adjusting device parameters. Interestingly, a large variation of recess depth has almost no effect on the threshold voltage when the recess depth is up to 500 nm, which indicates a good tolerance of the etching process in the fabrication. In addition to this, by using the short channel effect, we also analyze the reason why the threshold voltage conspicuously shifts towards the negative direction as the recess depth is reduced to less than 300 nm. Moreover, the proposed structure is feasible to broaden the high-field region and hence reduce the peak electric field intensity, which makes breakdown voltage be 78% higher than $V_B$ of the conventional MIS-HEMT. In addition, as the fabrication process of GTCE-HEMT is compatible with that of the conventional D-mode devices, this structure can realize the possibility of achieving the switch application and the E/D-mode logic circuit.

## References

[1] Khan M A, Kuznia J N, Bhattarai A R and Olson D T 1993 *Appl. Phys. Lett.* **62** 1786
[2] Wu Y F, Keller B P, Keller S, Kapolnek D, Kozodoy P, DenBaars S P and Mishra U K 1996 *Appl. Phys. Lett.* **69** 1438
[3] Ambacher O, Smart J, Shealy J R, Weimann N G, Chu K, Murphy M, Dimitrov R, Wittmer L, Stutzmann M, Rieger W and Hilsenbeck J 1999 *J. Appl. Phys.* **85** 3222

[4] Hikita M, Yanagihara M, Nakazawa K, Ueno H, Hirose Y, Ueda T, Uemoto Y and Tanaka T 2005 *IEEE Trans. Electron Dev.* **52** 1963

[5] Cao X A, Cho H, Pearton S J, Dang G T, Zhang A P, Ren F, Shul R J, Zhang L, Hickman R and Van Hove J M 1999 *Appl. Phys. Lett.* **75** 232

[6] Cai Y, Zhou Y, Lau K M and Chen K J 2006 *IEEE Trans. Electron Dev.* **53** 2207

[7] Feng Z H, Zhou R, Xie S Y, Yin J Y, Fang J X, Liu B, Zhou W, Chen K J and Cai S J 2010 *IEEE Electron Dev. Lett.* **31** 1386

[8] Khan M A, Chen Q, Sun C J, Yang J W, Shur M S and Park H 1996 *Appl. Phys. Lett.* **68** 514

[9] Mi M H, Zhang K, Chen X, Zhao S L, Wang C, Zhang J C, Ma X H and Hao Y 2014 *Chin. Phys. B* **23** 077304

[10] Kuroda M, Ishida H, Ueda T and Tanaka T 2007 *J. Appl. Phys.* **102** 093703

[11] Kuroda M, Ueda T and Tanaka T 2010 *IEEE Trans. Electron Dev.* **57** 368

[12] Fujiwara T, Keller S, Speck J S, DenBaars S P and Mishra U K 2012 *Phys. Status Solidi C* **9** 891

[13] Fujiwara T, Keller S, Higashiwaki M, Speck J S, DenBaars S P and Mishra U K 2009 *Appl. Phys. Express* **2** 061003

[14] Fujiwara T, Keller S, Speck J S, DenBaars S P and Mishra U K 2010 *Appl. Phys. Express* **3** 101002

[15] Fujiwara T, Yeluri R, Denninghoff D, Liu J, Keller S, Speck J S, DenBaars S P and Mishra U K 2011 *Appl. Phys. Express* **4** 096501.

[16] Wen Y H, He Z Y, Li J L, Luo R H, Xiang P, Deng Q Y, Xu G N, Shen Z, Wu Z S, Zhang B J, Jiang H, Wang G and Liu Y 2011 *Appl. Phys. Lett.* **98** 072108

[17] Lee J H, Jeong J H and Lee J H 2012 *IEEE Electron Dev. Lett.* **33** 1429

[18] Wang Y, Wang M J, Xie B, Wen C P, Wang J Y, Hao Y L, Wu W G, Chen K J and Shen B 2013 *IEEE Electron Dev. Lett.* **34** 1370

[19] Okada M, Saitoh Y, Yokoyama M, Nakata K, Yaegassi S, Katayama K, Ueno M, Kiyama M, Katsuyama T and Nakamura T 2010 *Appl. Phys. Express* **3** 054201

[20] Nie H, Diduck Q, Alvarez B, Edwards A P, Kayes B M, Zhang M, Ye G F, Prunty T, Bour D and Kizilyalli I C 2014 *IEEE Electron Dev. Lett.* **35** 939

[21] Oka T, Ueno Y, Ina T and Hasegawa K 2014 *Appl. Phys. Express* **7** 021002

[22] Zhao S L, Chen W W, Yue T, Wang Y, Luo J, Mao W, Ma X H and Hao Y 2013 *Chin. Phys. B* **22** 117307

[23] Karmalkar S and Mishra U K 2001 *IEEE Trans. Electron Dev.* **48** 1515

[24] Farahmand M, Garetto C, Bellotti E, Brennan K F, Goano M, Ghillino E, Ghione G, Albrecht J D and Ruden P P 2001 *IEEE Trans. Electron Dev.* **48** 535

[25] Fang Z Q, Claflin B, Look D C, Green D S and Vetury R 2010 *J. Appl. Phys.* **108** 063706

[26] ATLAS Device Simulation Software, Silvaco Int., Santa Clara, CA, USA, 2012

[27] Takashima S, Li Z D and Chow T P 2013 *IEEE Trans. Electron Dev.* **60** 3025

[28] Kim D S, Im K S, Kim K W, Kang H S, Kim D K, Chang S J, Bae Y, Hahm S H, Cristoloveanu S and Lee J H 2013 *Solid-State Electron.* **90** 79

[29] Koblmüller G, Chu R M, Raman A, Mishra U K and Speck J S 2010 *J. Appl. Phys.* **107** 043527

[30] Yao Y, He Z Y, Yang F, Shen Z, Zhang J C, Ni Y Q, Li J, Wang S, Zhou G L, Zhong J, Wu Z S, Zhang B J, Ao J P and Liu Y 2014 *Appl. Phys. Express* **7** 016502

[31] Yu E T and Manasreh M O 2002 *III–V Nitride Semiconductors Applications and Devices*, Vol. 16 (New York: Taylor and Francis Books) pp. 163–168

[32] F Bernardini, V Fiorentini and D Vanderbilt 1997 *Phys. Rev. B* **56** R10024

[33] Yu E T, Sullivan G J, Asbeck P M, Wang C D, Qiao D and Lau S S 1997 *Appl. Phys. Lett.* **71** 2794

[34] Ambacher O, Foutz B, Smart J, Shealy J R, Weimann N G, Chu K, Murphy M, Sierakowski A J, Schaff W J, Eastman L F, Dimitrov R, Mitchell A and Stutzmann M 2000 *J. Appl. Phys.* **87** 334

[35] Ambacher O, Smart J, Shealy J R, Weimann N G, Chu K, Murphy M, Schaff W J, Eastman L F, Dimitrov R, Wittmer L, Stutzmann M, W Rieger and Hilsenbeck J 1999 *J. Appl. Phys.* **85** 3222

[36] Keller S, Parish G, Fini P T, Heikman S, Chen C H, Zhang N, DenBaars S P, Mishra U K and Wu Y F 1999 *J. Appl. Phys.* **86** 5850

[37] Chang C Y, Wang Y L, Gila B P, Gerger A P, Pearton S J, Lo C F, Ren F, Sun Q, Zhang Y and Han J 2009 *Appl. Phys. Lett.* **95** 082110

[38] Kuraguchi M, Takada Y, Suzuki T, Hirose M, Tsuda K, Saito W, Saito Y and Omura I 2007 *Phys. Stat. Sol. A* **204** 2010

[39] Jessen G H, Fitch R C, Gillespie J K, Via G, Crespo A, Langley D, Denninghoff D J, Trejo M and Heller E R 2007 *IEEE Trans. Electron Dev.* **54** 2589

[40] Chow T P and Ghezzo M 1996 "SiC power devices", in *III–Nitride, SiC, and Diamond Materials for Electronic Devices*, eds. Gaskill D K, Brandt C D and Nemanich R J, *Material Research Society Symposium Proceedings*, 1996, Pittsburgh, PA, p. 69